# Thermal Characteristics of Fin-and-Tube Heat Exchanger Cooled By Natural Convection

**N. Kayansayan**
*Department of Mechanical Engineering, Dokuz Eylul University, Izmir, Turkey*

■ There are numerous instances where the heat transfer from a fin-and-tube heat exchanger to air takes place primarily via natural convection. The lack of data showing the effect of fin spacing, fin length, and Rayleigh number on the thermal performance of the exchanger prompted this experimentation. It was found that the interaction of the fin boundary layer with the tube base brought about a reduction in the Nusselt number and in the convection-conductance value of the finned surface relative to that found in the classical case of the long isolated cylinder. At Rayleigh numbers beyond the critical, the Nusselt number was quite insensitive to fin spacing and length, with the typical data spread being 5–10%. For a given temperature difference, the occurrence of an optimum fin spacing ratio is indicated.

**Keywords:** *natural convection, fin-and-tube exchanger, critical Rayleigh number, radial fins*

## INTRODUCTION

Natural convection heat exchange devices such as those employed in dissipating heat from refrigeration units to the surrounding still air or in the cooling of cylindrical electronic components may involve the interaction of buoyant streams individually induced by various surfaces that comprise the device. A proper formulation of natural convective heat transfer coefficients presents difficulties for a unit consisting of a bank of finned tubes as shown in Fig. 1. In addition to radiative heat interactions between the finned tubes and the casing wall, as the buoyancy-induced flow proceeds through the exchanger, successive merging and disruption of air plumes generated by the heated tubes will take place. This complex physical situation is the subject of the present work, in which the thermal performance of a single horizontal finned tube in still air was investigated experimentally.

The experiments were performed with a highly polished, isothermal horizontal cylinder serving as the host surface for the vertical circular fins, which were also polished to a mirrorlike finish. Three parameters were varied during the course of the experiments. One of these is fin spacing $s$. At each fixed spacing, the temperature difference between the cylindrical surface and the ambient was varied systematically, so that the cylinder Rayleigh number, Ra, ranged from about $10^5$ to $10^8$. Four values of the ratio of the fin diameter to the tube diameter, $D/d$ = 1.5, 2.0, 3.0, and 6.0, were used.

The main focus of the work is the determination of the heat transfer characteristics of the exchanger and the identification of the effects of fin–cylinder boundary layer interaction. Such interactions occur when the upward-moving natural convection boundary layer flow induced by two adjacent fins may interfere and impinge on the cylinder, which, in its own right, induces a buoyant upflow. In expressing cylinder Nusselt and Rayleigh numbers, the tube diameter $d$ is taken to be the characteristic dimension. This choice enables direct comparison of the present results with the literature information on single cylinders at identical conditions and also leads to a more compact correlation of the results. In recognition of the relatively low values of the natural convective heat transfer coefficient for surfaces situated in air, special precautions were taken to prevent extraneous heat loss due to conduction and radiation. Special features of the apparatus and the procedures used to ensure results of high accuracy are described in detail.

A search of the literature failed to reveal any published work related to the subject of this research. Studies related to systems of parallel or staggered fins attached to a vertical plate are well documented [1, 2]. In a review by Incropera [3], studies that deal with interactions between pin-fin arrays in air with and without shrouds are summarized.

## EXPERIMENTAL SETUP AND PROCEDURE

### Apparatus

A schematic diagram of the apparatus is presented in Fig. 2. The stainless steel heating element located at the center of the system is 24 mm in diameter and 600 ± 3 mm long and has a wall thickness of 4 mm. The tube accommodates a 15 mm diameter ceramic core with a spiral of four grooves/cm machined to a depth of 1.5 mm on its periphery. In the design of the heater, the choice of the heating wire was made to attain the highest

Address correspondence to Dr. N. Kayansayan, Department of Mechanical Engineering, Dokuz Eylul University, Bornova 35100, Izmir, Turkey.

*Experimental Thermal and Fluid Science* 1993; 7:177–188

0894-1777/93/$6.00

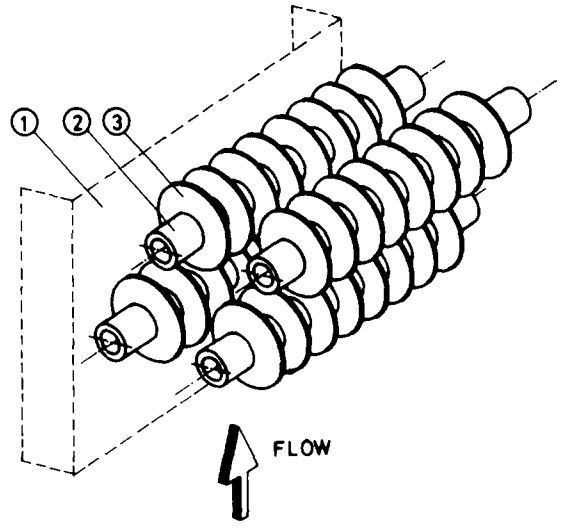


**Figure 1.** Sketch of a heat exchanger operated in the natural convection mode. *1*, Casing wall; *2*, heated tube; *3*, circular fin of constant thickness.

possible resistance and thereby to keep the electric current flow as small as possible. A nichrome wire, 10 m in length and 0.5 mm in diameter with resistivity of $10^{-4}$ ohm · cm, was installed in the ceramic grooves to provide uniform heating along the tube axis. To reduce possible extraneous heat loss by conduction, 0.5 mm diameter copper lead wires were used to deliver the power to the heater. For the same reason, the voltage tap wires used for measuring the voltage drop across the heating element were of 0.1 mm diameter constantan.

To facilitate the variation of fin spacing, pure aluminum collars of two different widths, 12.5 mm and 25 mm, were machined and polished on a lathe. Thus, with the outside diameters being 200, 150, 100, and 50 mm, a total of eight different types of cylindrical collars were constructed. Each collar has a central hole 24 mm in diameter bored with 0.1 mm tolerance, which ensures a snug fit around the heating tube, and a 2 mm hole drilled along the radial direction, which provides accommodation for a thermocouple wire to measure the surface temperature. Slots 5 mm deep by 10 mm wide machined on the central bore hole of the collars provide an internal housing channel for the thermocouple wires.

To secure a uniform temperature distribution along the fin surface, copper fins 2 mm thick, 300 mm in diameter, and having the same design features as the collars were employed in the experiments. The exposed faces of the fins were subjected to a polishing procedure that produced a surface finish that can be characterized as "highly polished" from the standpoint of thermal radiation properties.

As shown in Fig. 2, the exchanger assembly was compressed by bakelite nuts fitted on the ends of the stainless steel tubing; this gave good thermal contact between the collars and the fins. The ends of the assembly were completely insulated with a layer of styrofoam backed by wooden shrouds. The apparatus was mounted on a steel frame so that a minimum elevation of 50 cm from the ground level was provided for the free motion of air currents through the test section. In addition, the frame allowed rotation of the system about its axis to facilitate circumferential temperature measurements on the cylindrical surface.

## Instrumentation and Experimental Procedure

Figure 3 shows the fin layout and the thermocouple arrangement. The characteristics of the thermocouple wire, that is, small diameter and high sensitivity, were selected with a view to minimizing resolution of small temperature differences. This objective was fulfilled by 0.3 mm diameter fiberglass-coated copper-constantan wire that was specially calibrated for these experiments. Each test configuration was equipped with seven thermocouples. Six of these thermocouples were positioned along the cylindrical surface such that two were at a distance of $s/2$ from the ends of the exchanger and the others, at approximate intervals of $(n-2)s/5$, were at midsections of the collars. These thermocouples were so installed through the 2 mm openings of the aluminum collars and fixed to the surface with copper oxide cement that there was precise axial alignment along the fin-and-tube assembly. The seventh thermocouple measured the tip temperature of a fin at the midsection of the assembly. The temperature of the ambient air was sensed (and possible stratification detected) by a vertical array of three thermocouples. Being 50 cm apart in the vertical direction, these thermocouples were completely shielded with regard to the radiation from the apparatus. After passing through a scanner system, the thermocouple emf outputs were read by a 4.5-digit digital voltmeter that had been used in the thermocouple calibration. All thermocouple interfaces (ie, connectors and terminals) were maintained spatially isothermal by means of an enveloping aluminum block.

Power for the heater was provided by a regulated ac supply with a capacity of 2 kW and a stability of 0.5% over a 3-day period. The power circuitry involved an autotransformer for voltage control. All heater-related voltages and the current were measured with a digital voltmeter and an ammeter that had been calibrated with an ac/dc calibration standard, and both instruments had a rated accuracy of $\pm 0.2\%$ of the reading.

The experimental apparatus was situated in a laboratory of dimensions 4.3 m × 7.6 m × 3 m that possessed remarkable thermal isolation and stability characteristics. The laboratory is, in fact, a room within a room. Its walls, ceiling, and floor are each backed by a 20 cm thickness of cork, which provides excellent thermal isolation. There are no ducts, grills, vents, or heating pipes in the laboratory. Thermal stratification, even after long data runs, was negligible. To ensure the absence of disturbances in the laboratory, all instrumentation and power supplies were situated in a room adjacent to the laboratory.

In determining the effect of geometrical parameters on the heat transfer characteristics of the exchanger, many experiments were carried out on different dimensions (Table 1). Each data run was initiated by setting the heater power inputs at levels that would yield the desired surface-to-ambient temperature difference. Then an equilibration period of at least 8 h was allowed before any readings were made. In addition to the power consumption, the laboratory air, cylinder surface, and fin-tip temperatures were recorded. After rotating the fin-and-tube

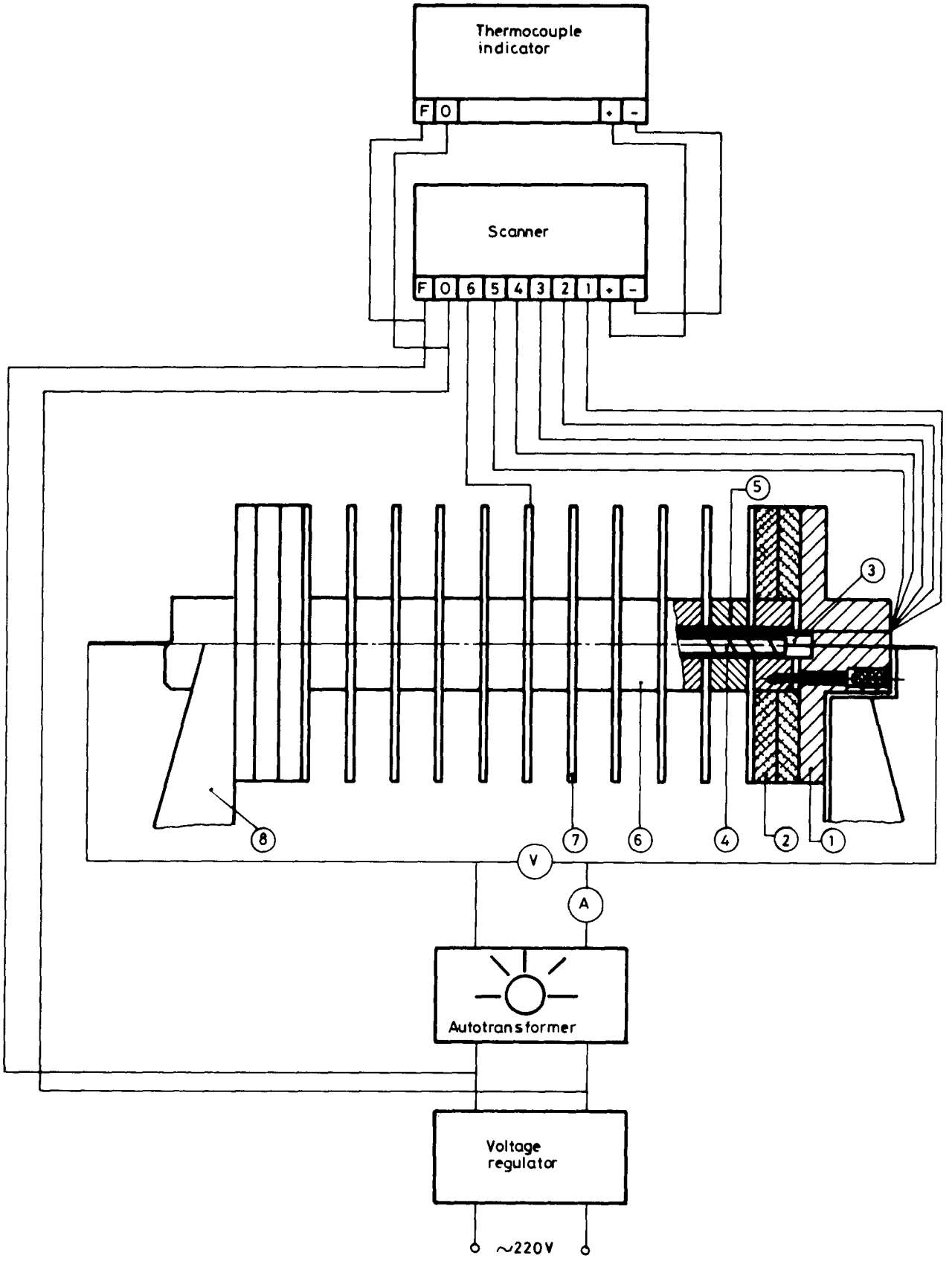


**Figure 2.** Schematic diagram of the experimental apparatus. *1*, Wood shroud; *2*, insulation; *3*, stainless steel tubing; *4*, ceramic core; *5*, thermocouple; *6*, collar; *7*, circular fin; *8*, steel frame.

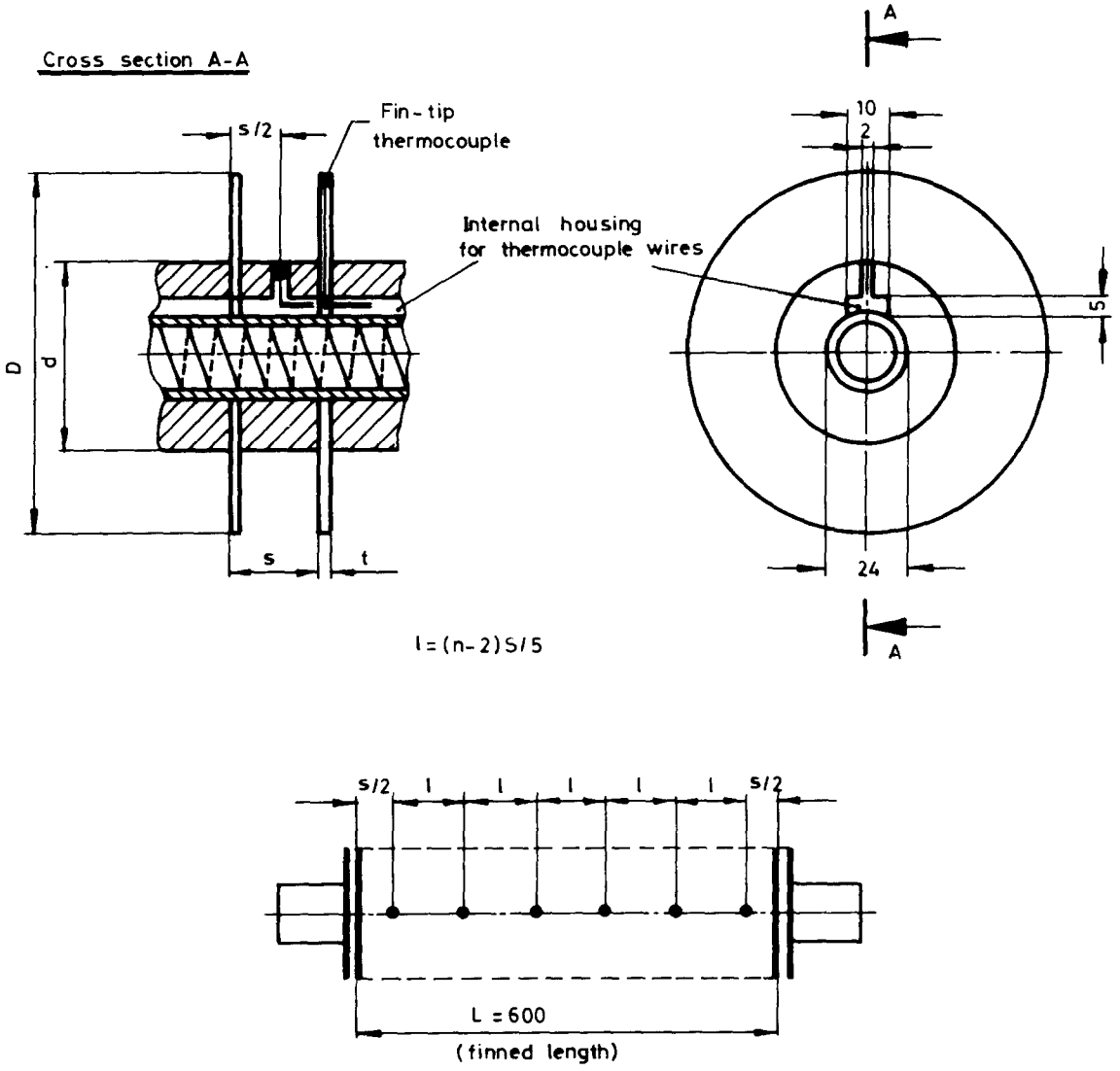


**Figure 3.** Exchanger characteristic geometry and thermocouple arrangement.

**Table 1.** Finned Tube Test Dimensions

| *Configuration Number* | *Fin Diameter D (mm)* | *Fin Thickness t (mm)* | *Tube Diameter d (mm)* | *Fin Spacing s (mm)* | *Number of Fins n* | *Exchanger Finning Factor α* |
|---|---|---|---|---|---|---|
| 1 | 300 | 2 | 200 | 12.5 | 49 | 11.090 |
| 2 | 300 | 2 | 200 | 25 | 25 | 5.925 |
| 3 | 300 | 2 | 200 | 50 | 13 | 3.531 |
| 4 | 300 | 2 | 200 | 100 | 7 | 2.268 |
| 5 | 300 | 2 | 200 | 200 | 4 | 1.638 |
| 6 | 300 | 2 | 150 | 37.5 | 17 | 5.305 |
| 7 | 300 | 2 | 150 | 75 | 9 | 3.031 |
| 8 | 300 | 2 | 150 | 150 | 5 | 1.893 |
| 9 | 300 | 2 | 100 | 12.5 | 49 | 16.707 |
| 10 | 300 | 2 | 100 | 25 | 25 | 8.606 |
| 11 | 300 | 2 | 100 | 50 | 13 | 4.555 |
| 12 | 300 | 2 | 100 | 100 | 7 | 2.529 |
| 13 | 300 | 2 | 50 | 12.5 | 49 | 71.855 |
| 14 | 300 | 2 | 50 | 25 | 25 | 36.438 |
| 15 | 300 | 2 | 50 | 50 | 13 | 24.011 |

assembly 60° about its axis and allowing sufficient time for the reinstatement of steady-state flow conditions, cylinder wall temperatures were recorded. Repeating the procedure for angular rotations of 120° and 180°, the circumferential variation of the wall temperatures was also detected. The power to the heater was systematically raised to change the averaged wall and ambient temperature difference $\Delta T$ from 10 K to 180 K by 5 K increments at low Rayleigh numbers and by 10 K increments at high Ra.

Note was taken of the degree of temperature deviations along the cylindrical surface. In principle, to establish identical flow conditions on the axial direction of the test exchanger, the measured longitudinal temperatures at a particular run should be equal. In experiments, specifically at high power inputs, the maximum temperature deviation was calculated to be 2.7% of the wall-to-ambient temperature difference $\Delta T$.

## DATA REDUCTION

The procedures used to determine the finned tube heat transfer coefficients, Nusselt numbers, and Rayleigh numbers from the thermocouple outputs, power input, and barometric pressure will now be described. The starting point of the data reduction procedure is the definition of the average heat transfer coefficient for the finned surface,

$$h = Q/\eta A(T_w - T_\infty) \tag{1}$$

where $Q$ is the rate of heat transfer by natural convection from the surface to the air, and $A$ is the total exposed surface area, including the fin-tip face, expressed as

$$A = \frac{\pi}{2}(n-1)d^2\left[\left(\frac{D}{d}\right)^2 + 2\frac{s}{d} + 2\left(\frac{n}{n-1}\cdot\frac{D}{d} - 1\right)\left(\frac{t}{d}\right) - 1\right] \tag{2}$$

In Eq. (1), $\eta$ represents the total surface temperature effectiveness [4] and is defined as

$$\eta = 1 - \frac{A_f}{A}(1 - \eta_f) \tag{3}$$

The average of six thermocouple readings on both longitudinal and circumferential directions was used to evaluate $T_w$ in Eq. (1).

The electric power input to the heater is equal to the sum of the rates of heat transfer from the exchanger assembly by natural convection and by radiation. If $E$ and $I$, respectively, denote the measured voltage and current for the heater and $Q_r$ is the radiation heat transfer from the cylindrical finned surface, then

$$Q = EI - Q_r \tag{4}$$

For all geometrical configurations, $Q_r$ accounts for a considerable portion of the input power $EI$. Depending upon the surface geometry, at the highest power inputs, calculations showed that $Q_r/EI$ varied in the range of 3–18%. Similarly, at the low power extreme, $Q_r/EI$ ranged between 35 and 70%. Considering the major role of radiation, especially at low power inputs, it was calculated with care for each case.

Due to the use of copper fins in the experiments, fin efficiencies above 90% are quite realistic for transferring heat to air via natural convection. If the fin-tip to ambient temperature difference, $\Delta T_{ft}$, is expressed as a percentage of $\Delta T$, then for most experiments deviations in the tip temperature difference were in the range of 6–14% of the base temperature difference $\Delta T$. At the geometrical configuration for which $D/d$ was 6.0 and only high power inputs, a maximum of 16% deviation was detected. Consequently, within acceptable engineering accuracy, the fins can be assumed to be at a uniform temperature, which is evaluated as the average of the base and tip values for the radiative heat loss analysis. It should be also noted that $T_\infty$ denotes both the temperature of the air and the temperature of the walls of the laboratory. Furthermore, the laboratory room closely fulfills all the requirements of a blackbody enclosure. Therefore, the radiant energy absorbed by the room is blackbody radiation.

With respect to the above experimental observations, all the fins are at identical thermal conditions, and, as shown in Fig. 4, an enclosure confined by two adjacent fins, the collar in between, and the imaginary black surface S4 complete the unit cell for radiation analysis. The radiant energy flux streaming through the cell can be regarded as having two components. One of these stems from the black surface S4. The other stems from the fin-tip surface owing to a temperature different from that of the room. These two contributions to $Q_r$ are designated as $Q_{r1}$ and $Q_{r2}$, respectively. The heat loss through surface S4 is

$$Q_{r1} = \pi D(s-t)(n-1)q_4 \tag{5}$$

where $q_4$ represents the net radiant flux through surface

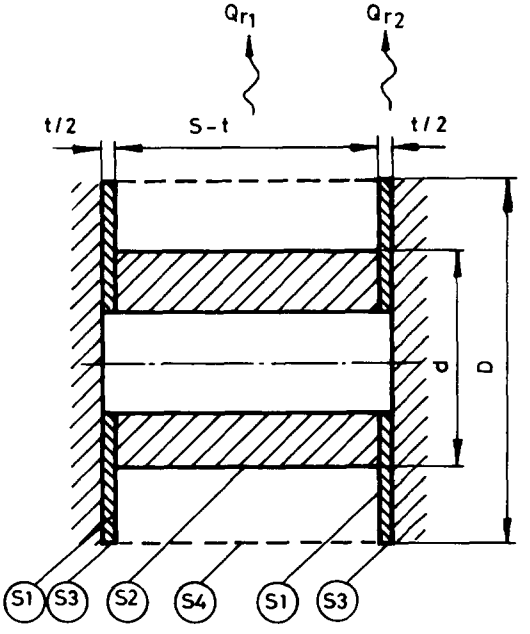


**Figure 4.** Unit enclosure for radiative heat transfer analysis.

S4. The details in relating this flux to the measured properties are presented in the Appendix. Furthermore, the radiation exchange between the fin-tip surface, surface S3 in Fig. 4, and the room is

$$Q_{r2} = \pi Dtn\sigma\epsilon_{ft}(T_{ft}^4 - T_\infty^4) \quad (6)$$

Equations (5) and (6) can now be added together to yield $Q_r$. Figure 5 shows the variation of $Q_r/EI$ versus the temperature difference between the wall surface and the ambient for typical values of fin-to-tube diameter and spacing ratios. The general distribution in this illustration indicates that an increase in the temperature difference and/or in the diameter ratio $D/d$ dramatically decreases the radiation losses, and the curve becomes quite flat in the range where $\Delta T > 25$ K. It is also evident from Fig. 5 that the fin spacing is the dominant factor at high diameter ratios. For $D/d = 6.0$, changing the spacing ratio $s/d$ from 0.25 to 1.00 increases the radiation losses by a factor of 4; however, for $D/d = 1.5$, the increase is a factor of 2.

With the determination of $Q_r$, the convective heat transfer rate $Q$ follows from Eq. (4), and the heat transfer coefficient $h$ is then evaluated from Eq. (1). The $h$ values will be reported in dimensionless form via the Nusselt numbers, $\mathrm{Nu} = hd/k$. The results will be parameterized by the Rayleigh number, $\mathrm{Ra} = g\beta\rho^2 c_p d^3(T_w - T_\infty)/\mu k$, and by the modified Rayleigh number,

$$Ra^* = Nu \cdot Ra \quad (7)$$

Aside from $\beta$, the thermophysical properties contained in the Nusselt and Rayleigh number expressions were computed at a reference temperature, $T_{ref}$, suggested by Sparrow and Gregg [5],

$$T_{ref} = T_w - 0.38(T_w - T_\infty) \quad (8)$$

and $\beta = 1/T_\infty$. The measured barometric pressure was used in the determination of the density $\rho$. The uncertainties in the measured properties were estimated to be as in Table 2. The method of Kline and McClintock [6] was employed in evaluating the uncertainties of the experimental results. In the analysis, the uncertainty arising from the surface area of the test exchanger was ignored, and the overall uncertainty in the radiative heat transfer was dominated by the uncertainties in variables $T_w$, $T_{ft}$, $T_\infty$, and $\epsilon$ [7]. Then, combining the uncertainty contributions made by the radiation and the total power input, the uncertainty in convective heat transfer was estimated. For moderate wall-to-ambient temperature difference ($\Delta T \sim 70$ K), the radiation heat losses were found to be within 6% and the heat transfer coefficients within 7% of the reported values.

## RESULTS AND DISCUSSION

Figure 6 presents the Nusselt number results as a function of the modified Rayleigh number for fin diameter ratios $D/d = 1.5, 2.0, 3.0, 6.0$ and for spacing ratios $s/d = 0.25$, 0.5, and 1.0. In this figure, a direct comparison of Nusselt numbers at a particular Ra* value indicates that as the diameter ratio increases, the heat transfer coefficients also increase. This is basically attributed to the up-moving boundary layer flow induced by fins. At large fin diameter

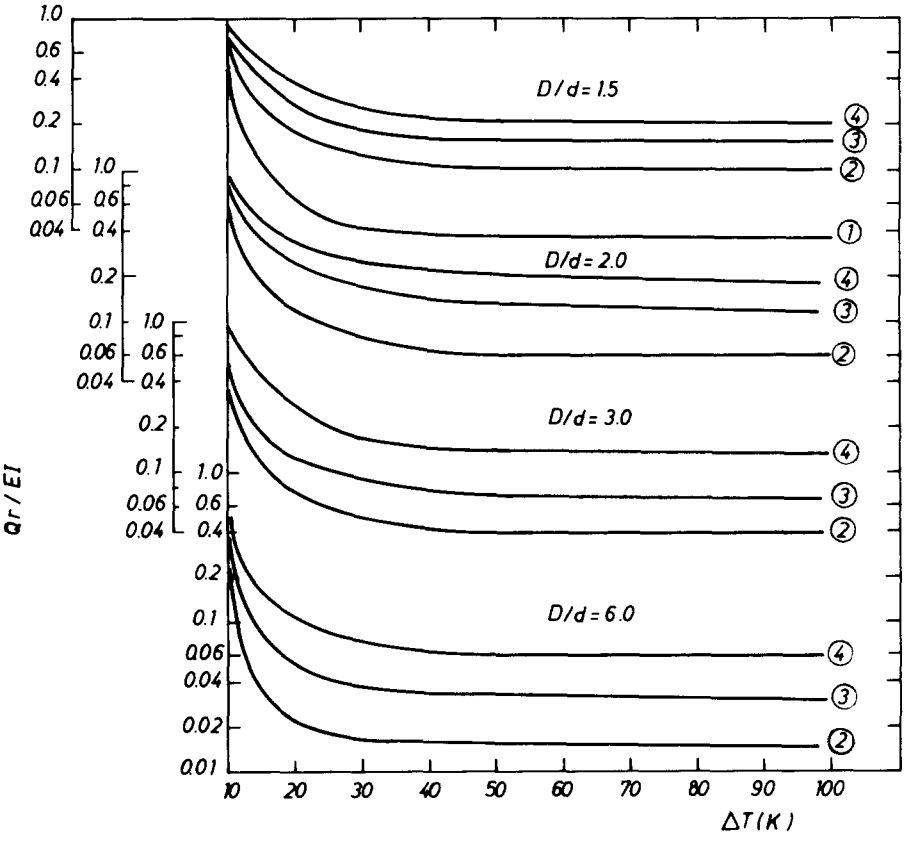


**Figure 5.** Effect of geometrical parameters of the finned tube on radiative heat loss fraction. $\gamma$: (1) 0.0625; (2) 0.25; (3) 0.50; (4) 1.00.

ratios, the existence of such an oncoming flow is stronger and reinforces the buoyant flow that is induced by the tube base itself. Thus, the augmented velocity field should give rise to higher heat transfer coefficients.

In direct conflict with the velocity-related enhancement is the preheating effect due to fins. Owing to the heat transfer from the fin to the air that passes along it, the temperature of the fin-induced airflow that arrives at the cylinder surface is higher than the ambient temperature. Thus, for identical flow conditions, the effective finned tube-to-air temperature difference is less than the temperature difference between the bare tube surface and the ambient. This behavior then tends to degrade the heat transfer coefficients. The extent of the degradation should be greater when the fin diameter ratio is larger, since the preheating effect of the fin increases with its diameter.

Since both the aforementioned opposing effects are especially stronger at high Rayleigh numbers, there should be a limit to the increase of heat transfer coefficients. It is evident from Fig. 6 that the data points for all diameter ratios approach asymptotically to the horizontal cylinder results. There are a number of competing correlations in the literature for horizontal cylinders. Three of the most accepted correlations have been evaluated for the operating conditions of the present experiments and compared with the present findings. These include those of Churchill and Chu ([8], Eq. (10)), Fand et al. ([9], Eq. (17)), and Morgan ([10], Table 2). The Churchill-Chu correlation, as restated with respect to modified Rayleigh number, is plotted in Fig. 6 and displays an upper bound to the present findings.

**Table 2.** Experimental Uncertainties

| *Property* | *Uncertainty* | *Range* |
|---|---|---|
| Surface temperature | ±0.3 K | 303–443 K |
| Ambient temperature | ±0.5 K | 293–298 K |
| Wall temperature difference | ±0.5 K | 10–180 K |
| Power input | ±0.5 W | 10–100 W |
| | ±2.2 W | 100–780 W |
| Total emissivity | ±0.002 | 0.04–0.072 |

The general sensitivity of Nu values to $D/d$ is worthy of special note, and Fig. 7 may be examined in this regard. Here, Ra* = Nu × Ra data for a fin diameter of 3.0 are plotted as a function of Rayleigh number. An interesting feature of this illustration is the existence of "discrete transitions." In the classical case of natural convection along a vertical plate, the local wall heat transfer versus the Grashof number representation of the experimental data of Tsuji and Nagano [11] exhibits the occurrence of a secondary discontinuity when the flow changes from laminar to transitional. In the present case, however, the flow along the fin is superimposed on the flow around the cylinder. Besides, there is a merging of the streams generated by the fin and by the tube base. Consequently, the thermal behavior of the resulting flow differs substantially from that of the isolated plate, and such discontinuities are not detected in the experiments. An ad hoc method that has been verified to be successful [12, 13] is implemented in locating the transition points. The method considers a change in the slope of a linear curve produced

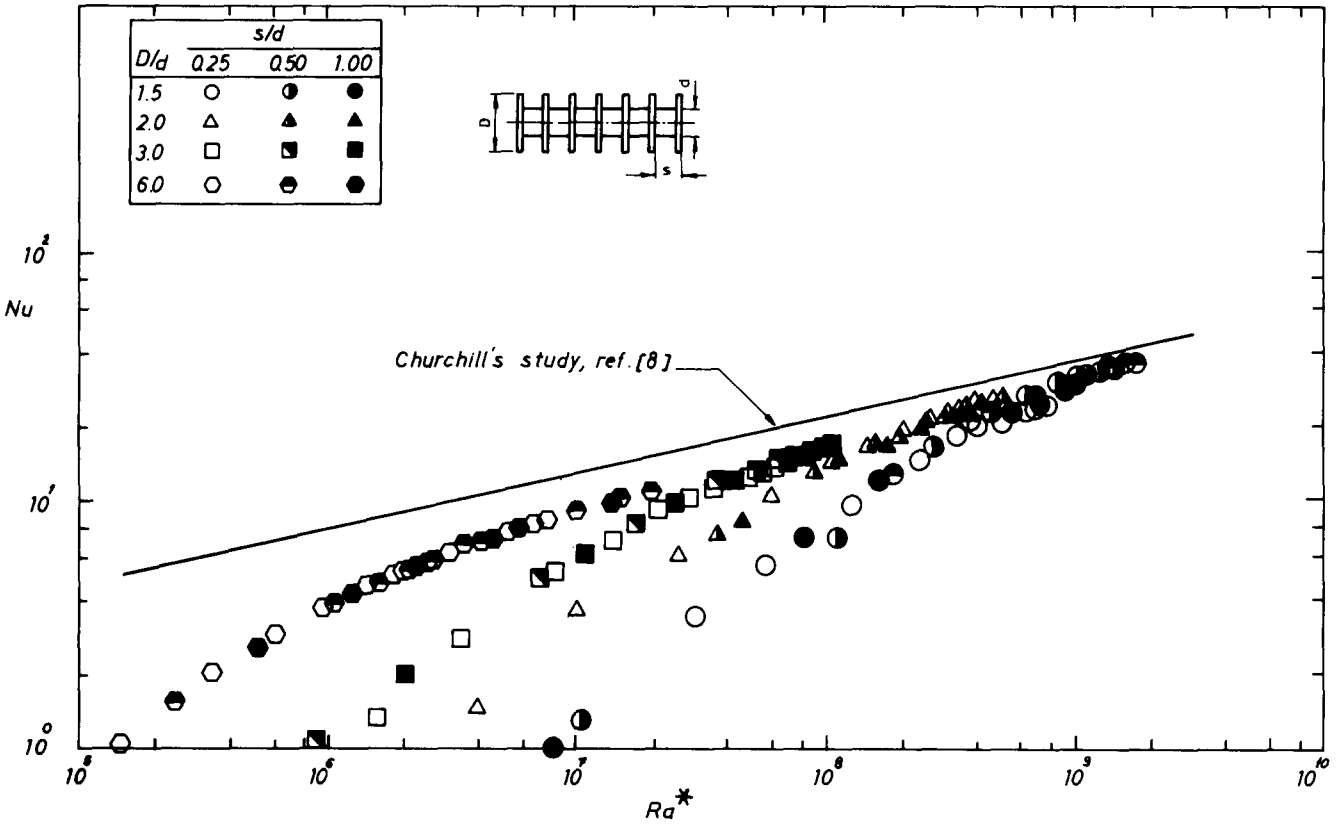


**Figure 6.** Finned tube natural convective heat transfer data and comparison with horizontal cylinder results.

**Table 3.** Critical Rayleigh Numbers for Discrete Transitions in Heat Flux for $0.25 \leq s/d \leq 1.00$

| $D/d$ | $Ra_{cr}$ | $(D/d)^3 \times Ra_{cr}$ |
|---|---|---|
| 1.50 | $1.780 \times 10^7$ | $6.007 \times 10^7$ |
| 2.00 | $0.775 \times 10^7$ | $6.200 \times 10^7$ |
| 3.00 | $0.230 \times 10^7$ | $6.210 \times 10^7$ |
| 6.00 | $0.028 \times 10^7$ | $6.048 \times 10^7$ |

in determining the transition. The critical Rayleigh numbers at the transitions are summarized in Table 3. As shown in this table, for spacing ratios in the range 0.25–1.0, the term $\lambda^3 \mathrm{Ra}_{cr}$, with a deviation of $\mp 2\%$, can be stated to be constant for all diameter ratios and approximated as

$$\lambda^3 \cdot \mathrm{Ra}_{cr} = 6.11 \times 10^7 \tag{9}$$

The significance of the transition is that no fin boundary layer interference occurs at Rayleigh numbers above the critical value, and the data points for all geometric parameters cluster on a single line. As shown in Fig. 8 for $\mathrm{Ra} > \mathrm{Ra}_{cr}$, the effect of the fin diameter and spacing on Nusselt number becomes undetectable in the data presentation. Then a single equation relating the two principal parameters is determined from a least-squares curve fit and is given by

$$\mathrm{Nu} = 0.081\,\mathrm{Ra}^{0.336} \tag{10}$$

This relation is found to be valid for the ranges of parameters indicated by $D/d = 1.5$–$6.0$, $s/d = 0.25$–$1.0$, and $\mathrm{Ra} > \mathrm{Ra}_{cr}$. In Eq. (10), the exponent is very close to Morgan's result [10] and signals, as expected, the lessened influence of fin–tube interaction.

To determine the effect of fin spacing on the performance of the heat exchanger, the test data were also plotted in the form shown in Fig. 9. This figure shows two distinct ordinates plotted against the fin spacing ratio at a temperature difference $\Delta T = 67$ K. The ordinate at the left, used for the solid curves, is the finned surface convection conductance value divided by the bare tube convection conductance value,

$$\phi = \eta hA/(hA)_0 \tag{11}$$

The ordinate at the right, to which the dashed curves correspond, represents the exchanger finning factor $\alpha$ and expresses the ratio of the total finned surface area exposed to air to the plain tube area:

$$\alpha = A/A_0 \tag{12}$$

In Fig. 9, as the fin density increases, that is, $s/d \ll 1$, the convection–conductance ratio does not increase in the same manner as the finning factor does. This result is indicated by the variation of the parameter $\phi/\alpha$ at the top of the same figure. As the spacing ratio increases, a smaller fraction of the tube base will be affected by the fin boundary layer and a relevant enhancement in $\phi$ is noted. It may also be seen that for any $s/d$ value the heat transfer from the finned surface will never be as great as that which would be obtained from a plain tube of equal diameter and surface area; that is, if $\alpha = 1$, then $\phi < 1$ in $\phi/\alpha$ vs. $s/d$ representation.

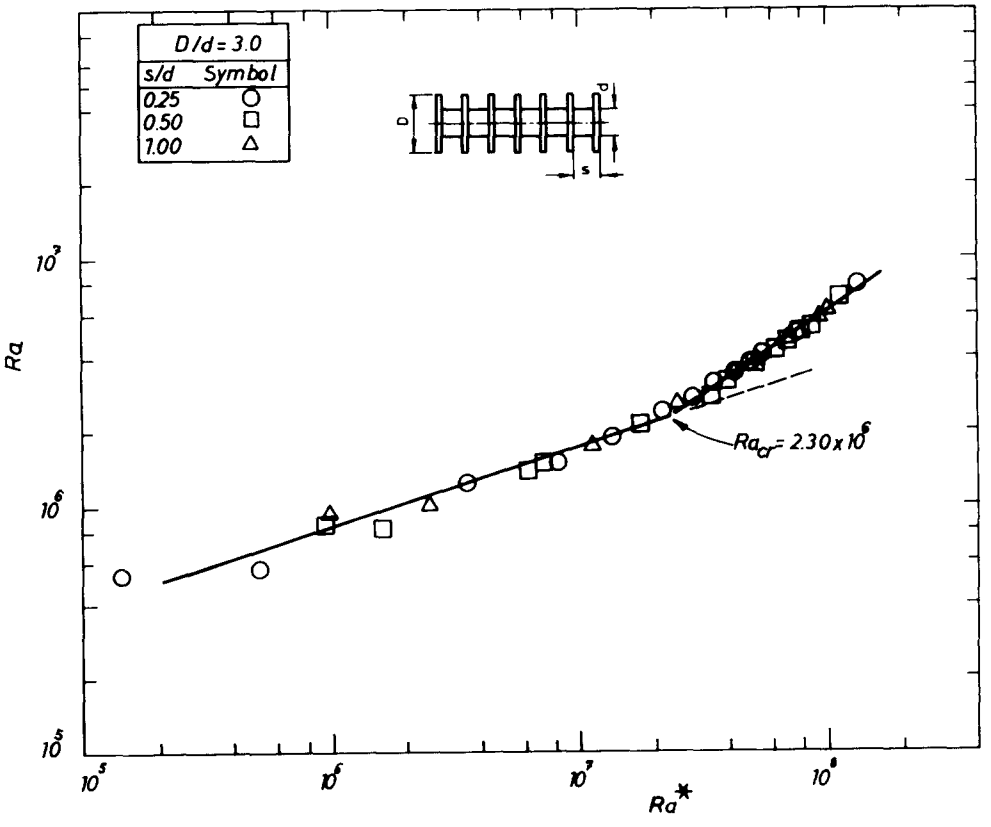


**Figure 7.** Discrete transition in natural convective heat flux for horizontally oriented finned tube.

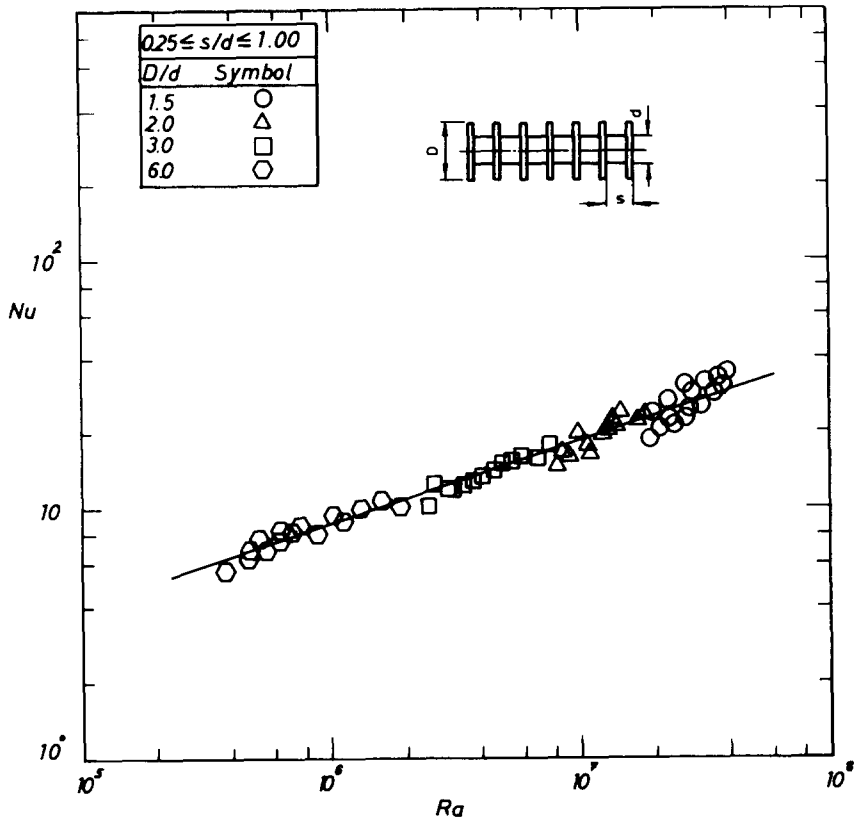


**Figure 8.** Average Nusselt number results for spacing ratios ranging from 0.25 to 1.00 and for Rayleigh numbers above the critical.

It is of value to be able to evaluate the total heat flow from the finned surface for a particular fin-and-tube geometry and temperature difference $\Delta T$. Figure 10 should be observed in this regard. The "effective" heat transfer coefficient $h_e$, which represents the combined convection and radiation heat flux streaming through the finned surface per unit temperature difference, defines the effective Nusselt number, $h_e d/k$, as the ordinate in Fig. 10. At a predetermined Rayleigh number value, the convective Nusselt number can be estimated by using Fig. 6 or Eq. (10) provided that the surface geometric parameters are in the ranges specified in the present study. Then Fig. 10 yields the heat transfer coefficient required for calculating the total heat flow rate. Figure 10 shows that the data are scattered at low Nu values. This behavior is attributed to the dominance of the radiative heat transfer in the dissipated heat rate at low temperatures. It may be seen from Fig. 5 that for $\Delta T < 25$ K the portion of the total heat input carried away by radiation drops from 70% to 10% and strongly depends on the fin-and-tube configuration. However, due to the fairly constant and small contribution of radiation at high $\Delta T$ values, $\Delta T > 30$ K, the data points for Nu vs. $\mathrm{Nu}_e$ merge to a single line.

## PRACTICAL SIGNIFICANCE

Arrays of horizontal finned tubes are used in numerous storage devices. Heat transfer engineering designers prefer the natural convection mode because it is more reliable due to the elimination of the cooling fluid circulation circuit. This study analyzes the basic mechanism of heat transfer from such devices. To achieve effective cooling from the finned surface, the exchanger should operate at Rayleigh numbers above the critical, which is defined in Eq. (9). The natural convective heat transfer from an untested exchanger may be computed by Eq. (10) provided that the geometric parameters and the Rayleigh numbers lie in the ranges specified. Tube surfaces with densely located fins should be avoided. To achieve the maximum cooling rate at a particular wall—ambient temperature difference, the criterion $0.25 \leq s/d \leq 0.50$ should be implemented.

## CONCLUSION

In the experiments reported here, three physical parameters were varied with a view to analyzing the natural convection characteristics of a horizontally oriented isothermal heat exchanger equipped with constant-thickness circular fins. The varied parameters included the fin spacing ratio, which ranged from 0.0625 to 1.0, the fin diameter ratio in the range 1.5–6.0, and the surface–fluid temperature difference, that is, the cylinder Rayleigh number. To provide equitemperature surfaces, copper fins and aluminum collars were used as the cylindrical surface for all the experiments. The data, which cover the Rayleigh number range from $10^5$ to $5 \times 10^7$, are appropriate for most applications of this type of extended surface when heat is transferred to air by natural convection.

The Nusselt number tends to be enhanced by the fin-induced approach flow and to be degraded by the fin-related preheating of the approach flow. The degrading effect is considerable at low Rayleigh numbers. At high Ra values, however, the net balance between these two conflicting effects was found to be insensitive to all the

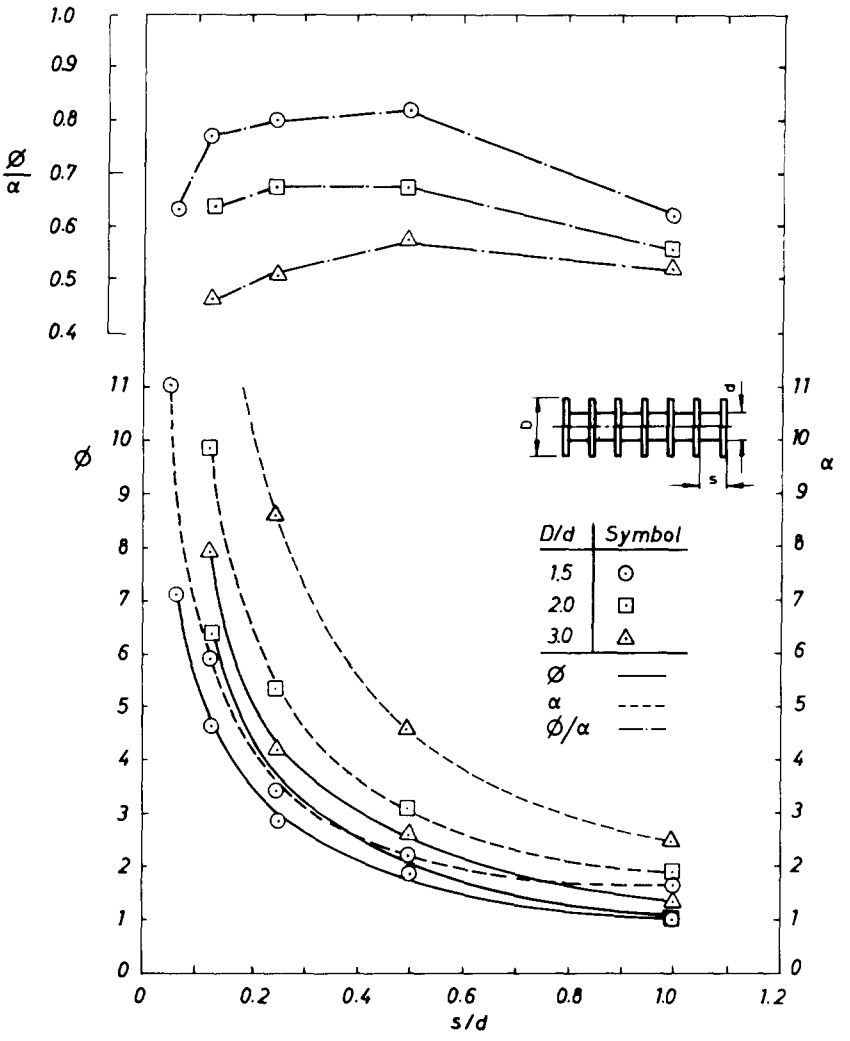


**Figure 9.** Effect of fin spacing on convection–conductance at a temperature difference of 67 K.

varied geometrical parameters. The critical Rayleigh number marked the transition to this insensitivity, and an abrupt change of slope in the Ra* vs. Ra presentation was noticed.

The net effect of the presence of the fins is to degrade the cylinder Nusselt number, as witnessed by the fact that the Nusselt numbers for the finned tube are lower than those for a single isolated cylinder. The test data for Rayleigh numbers above the critical value are correlated by Eq. (10), which represents the data with a $\mp 10\%$ deviation.

On the basis of identical surface area and temperature difference, the thermal behavior of the finned tube is compared with that of a horizontal tube. It is shown that convective heat transfer does not increase directly with increases in fin surface area. There is an optimum fin spacing for any fin diameter ratio, above or below which there is a reduction in convection–conductance. Depending upon the temperature difference, the optimum spacing radio $s/d$ lies between 0.25 and 0.50.

## APPENDIX

Referring to the enclosure in Fig. 4, where the hypothetical surface S4 simulates the surroundings, the following assumptions are made for the radiative heat exchange analysis:

1. The absolute temperature of each individual surface is uniform.
2. The hemispherical total emissivity of a surface depends only on the temperature of that particular surface.
3. The radiant energy is emitted and reflected diffusely.

The net radiative heat exchange between surfaces S1, S2, and S4 can be expressed as

$$q_{14} = F_{14}(q_{0,1} - \sigma T_\infty^4) \tag{A1}$$

$$q_{24} = F_{24}(q_{0,2} - \sigma T_\infty^4) \tag{A2}$$

Then the net radiant flux through surface S4 is

$$q_4 = 2q_{14} + q_{24} \tag{A3}$$

The radiosities $q_{0,1}$ and $q_{0,2}$ are obtained from the heat balance equations for surfaces S1 and S2. It follows that

$$\frac{\epsilon_1}{1-\epsilon_1}(\sigma T_1^4 - q_{0,1}) + F_{12}(q_{0,2} - q_{0,1}) + F_{14}(\sigma T_\infty^4 - q_{0,1}) + F_{13}(q_{0,3} - q_{0,1}) = 0 \tag{A4}$$

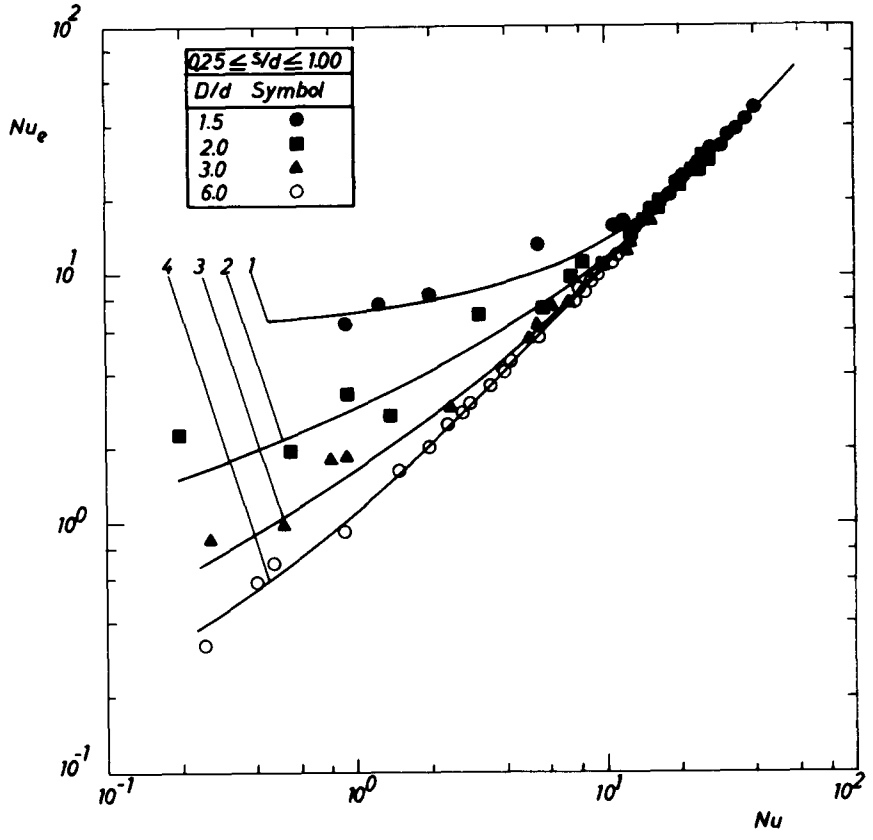


**Figure 10.** Finned tube total heat rate versus natural convection cooling rate. λ: (1) 1.5; (2) 2.0; (3) 3.0; (4) 6.0.

$$\frac{\epsilon_2}{1-\epsilon_2}(\sigma T_2^4 - q_{0,2}) + F_{21}(q_{0,1} - q_{0,2}) + F_{23}(q_{0,3} - q_{0,2}) + F_{24}(\sigma T_\infty^4 - q_{0,2}) = 0 \quad \textbf{(A5)}$$

For the particular enclosure under study, $q_{0,1} = q_{0,3}$ and $F_{23} = F_{21}$, Eqs. (A4) and (A5) can be simplified accordingly and rearranged to yield $q_{0,1}$ and $q_{0,2}$. Substituting the resulting expressions into Eqs. (A1) and (A2), the radiative heat flux through surface S4 becomes

$$q_4 = KT_1^4 + MT_2^4 - NT_\infty^4 \quad \textbf{(A6)}$$

where $T_1$, $T_2$, and $T_\infty$ are the respective absolute temperatures of the fin, the tube surface, and the surroundings. $K$, $M$, and $N$ are functions of the exchanger geometry, the surface emissivities, and the angle factors and are expressed as

$$K = \frac{2\sigma\epsilon_1}{1-\epsilon_1}\left(\frac{YF_{14} + F_{21}F_{24}}{Z}\right) \quad \textbf{(A7)}$$

$$M = \frac{\sigma\epsilon_2}{1-\epsilon_2}\left(\frac{XF_{24} + 2F_{14}F_{12}}{Z}\right) \quad \textbf{(A8)}$$

and

$$N = \sigma[XY(2F_{14} + F_{24}) - (XF_{24}^2 + 2YF_{14}^2) - 2F_{14}(F_{12}F_{24} + 2F_{12}F_{21} + F_{21}F_{24})]/Z \quad \textbf{(A9)}$$

where

$$X = \frac{\epsilon_1}{1-\epsilon_1} + F_{12} + F_{14} \quad \textbf{(A10)}$$

$$Y = \frac{\epsilon_2}{1-\epsilon_2} + 2F_{21} + F_{24} \quad \textbf{(A11)}$$

$$Z = XY - 2F_{21}F_{12} \quad \textbf{(A12)}$$

$\sigma$ is the Stefan-Boltzmann constant, and $\epsilon_1$, $\epsilon_2$ are the respective emissivities of the fin and tube surfaces and are determined experimentally by the Radiation Measurement System of the Institute. The range of the measured $\epsilon$ values is given in Table 2. The emissivity at a specified surface temperature is determined by interpolating the measured $\epsilon$ values. The $F$ factors in Eqs. (A7)–(A12) can be calculated from the configuration factor algebra. The following relations are used in computing the shape factors $F_{44}$ and $F_{42}$ [14]:

$$F_{44} = 1 - \frac{1}{\lambda} + \frac{2}{\pi\lambda}\arctan\left(2\frac{\sqrt{\lambda^2-1}}{\tau}\right) - \frac{\tau}{2\pi\lambda}\left[4\frac{\sqrt{\lambda^2+\tau^2}}{\tau}\arcsin \times\left(\frac{4(\lambda^2-1) + (\tau^2/\lambda^2)(\lambda^2-2)}{\tau^2 + 4(\lambda^2-1)}\right)\right.$$

$$-\arcsin\left(\frac{\lambda^2-2}{\lambda^2}\right)+\frac{\pi}{2}\left(\frac{\sqrt{4\lambda^2+\tau^2}}{\tau}-1\right)\Bigg] \quad \textbf{(A13)}$$

$$F_{42}=\frac{1}{\lambda}-\frac{1}{\pi\lambda}\left\{\arccos\left(\frac{\psi}{\nabla}\right)-\frac{1}{2\pi}\times\left[[(\nabla+2)^2-(2\lambda)^2]^{1/2}\arccos\left(\frac{\psi}{\lambda\Delta}\right)+\psi\arcsin\left(\frac{1}{\lambda}\right)-\frac{\pi\nabla}{2}\right]\right\} \quad \textbf{(A14)}$$

where $\lambda = D/d$, $\tau = 2(s-t)/d$, $\nabla = \tau^2 + \lambda^2 - 1$, and $\psi = \tau^2 - \lambda^2 + 1$. Moreover,

$$\sum_{j=1}^{4} F_{ij} = 1, \qquad i = 1,2,3,4 \quad \textbf{(A15)}$$

with the restriction that for $i \neq 4$, if $i = j$, then $F_{ij} = 0$, provide additional equations sufficient for estimating the shape factors of the enclosure.

I wish to express my appreciation to the administrative personnel of TEBA, Solar Collectors Manufacturing Inc., for their financial and technical support in the development of the experimental facility.

## NOMENCLATURE

- $A$ heat transfer surface area, $m^2$
- $c_p$ specific heat at constant pressure, $kJ/(kg \cdot K)$
- $D$ fin diameter, m
- $d$ tube base diameter, m
- $E$ voltage across the heating element, V
- $F$ angle factor, dimensionless
- $g$ gravitational acceleration, $m/s^2$
- $h$ heat transfer coefficient, $W/(m^2 \cdot K)$
- $I$ current through the heating element, A
- $k$ thermal conductivity, $W/(m \cdot K)$
- Nu Nusselt number ($= hd/k$), dimensionless
- $n$ number of fins, dimensionless
- $Q$ natural convection heat transfer rate from the finned tube, W
- $Q_r$ radiation heat transfer rate from the finned tube, W
- $q$ heat flux, $W/m^2$
- $q_{0,i}$ radiosity of $i$th surface, $W/m^2$
- Ra Rayleigh number $[= g\beta\rho^3 c_p d^2 (T_w - T_\infty)/\mu k]$, dimensionless
- Ra* modified Rayleigh number [Eq. (7)], dimensionless
- s fin spacing, m
- $T$ temperature, K
- $\Delta T$ temperature difference $T_w - T_\infty$, K
- $t$ fin thickness, m

### Greek Symbols

- $\alpha$ exchanger finning factor [Eq. (12)], dimensionless
- $\beta$ volumetric coefficient of thermal expansion, $K^{-1}$
- $\Delta$ difference
- $\epsilon$ surface emissivity, dimensionless
- $\gamma$ fin spacing ratio ($= s/d$), dimensionless
- $\lambda$ fin diameter ratio ($= D/d$), dimensionless
- $\eta$ efficiency, dimensionless
- $\mu$ dynamic viscosity, $kg/(m \cdot s)$
- $\rho$ density, $kg/m^3$

### Subscripts

- cr critical
- $e$ effective
- $f$ fin
- ft fin tip
- $r$ radiation
- ref reference
- $w$ wall
- 0 bare-tube conditions
- $\infty$ ambient conditions

## REFERENCES

1. Bar-Cohen, A., and Rohsenow, W. M., Thermally Optimum Spacing of Vertical Natural Convection Cooled, Parallel Plates, *ASME J. Heat Transfer*, **106,** 116–123, 1984.
2. Guglielmini, G., Nannei, E., and Tanga, G., Natural Convection and Radiation Heat Transfer from Staggered Vertical Fins, *Int. J. Heat Mass Transfer*, **30,** 1941–1948, 1987.
3. Incropera, F. P., Convection Heat Transfer in Electronic Equipment Cooling, *ASME J. Heat Transfer*, **110,** 1097–1111, 1988.
4. McQuiston, F. C., and Parker, J. D. *Heating, Ventilating, and Air Conditioning—Analysis and Design*, 3rd ed., pp. 555–562, Wiley, New York, 1988.
5. Sparrow, E. M., and Gregg, J. L., The Variable Fluid Property Problem in Free Convection, *ASME Trans.* **80,** 878–886, 1958.
6. Kline, S. J., and McClintock, F. A., Describing Uncertainties in Single-Sample Experiments, *Mech. Eng.*, **75,** 3–8, 1953.
7. Moffat, R. J., Describing the Uncertainties in Experimental Results, *Exp. Thermal Fluid Sci.*, **1,** 3–17, 1988.
8. Churchill, S. W., and Chu, H. H. S., Correlating Equations for Laminar and Turbulent Free Convection from a Horizontal Cylinder, *Int. J. Heat Mass Transfer*, **18,** 1049–1053, 1975.
9. Fand, R. M., Morris, E. W., and Lum, M., Natural Convection Heat Transfer from Horizontal Cylinders to Air, Water, and Silicone Oils for Rayleigh Numbers Between $3 \times 10^2$ and $2 \times 10^7$, *Int. J. Heat Mass Transfer*, **20,** 1173–1184, 1977.
10. Morgan, V. T., The Overall Convective Heat Transfer from Smooth Circular Cylinders, *Adv. Heat Transfer*, **11,** 199–264, 1975.
11. Tsuji, T., and Nagano, Y., Velocity and Temperature Measurements in a Natural Convection Boundary Layer Along a Vertical Flat Plate, *Exp. Thermal Fluid Sci.*, **2,** 208–215, 1989.
12. Malkus, W. V. R., Discrete Transitions in Turbulent Convection, *Proc. Roy. Soc. Lond. Ser. A*, **225,** 185–195, 1975.
13. Kulacki, F. A., and Richards, D. E., Natural Convection in Plane Layers and Cavities with Volumetric Energy Sources, in *Natural Convection: Fundamentals and Applications*, S. Kakac, W. Aung, and R. Viskanta, Eds., pp. 179–225, Hemisphere, Washington, D.C., 1985.
14. Siegel, R., and Howell, J. R., *Thermal Radiation Heat Transfer*, pp. 783–789, McGraw-Hill, New York, 1972.

Received November 17, 1992; revised April 1, 1993